Received: 1 July 2019 | Accepted: 6 December 2019

DOI: 10.1002/joc.6453

RESEARCH ARTICLE

International Journal of Climatology RMetS

The role of ENSO flavours and TNA on recent droughts over Amazon forests and the Northeast Brazil region

Juan C. Jimenez[1] | **Jose A. Marengo**[2] | **Lincoln M. Alves**[3] | **Juan C. Sulca**[4] | **Ken Takahashi**[5] | **Samantha Ferrett**[6] | **Matthew Collins**[7]

[1]GCU/IPL Catedratico Jose Beltran, University of Valencia, Paterna, Valencia, Spain

[2]CEMADEN, São José dos Campos - SP, Brazil

[3]INPE, CCST, São José dos Campos, Brazil

[4]Instituto Geofísico del Perú (IGP), Lima, Peru

[5]SENAMHI, Lima, Peru

[6]National Centre for Atmospheric Sciences, University of Reading, Reading, UK

[7]University of Exeter, Exeter, UK

Correspondence
Juan C. Jimenez, University of Valencia, GCU/IPL Catedratico Jose Beltran, 46980 Paterna, Valencia, Spain.
Email: jcjm@uv.es

Funding information
FAPESP, Grant/Award Number: 2014/50848-9; National Coordination for High-Level Education and Training (CAPES), Grant/Award Number: 16/2014; National Institute of Science and Technology for Climate Change Phase 2 under CNPq, Grant/Award Number: 465501/2014-1

Abstract

Amazon tropical forests and the semiarid Northeast Brazil (NEB) region have registered very severe droughts during the last two decades, with a frequency that may have exceeded natural climate variability. Severe droughts impact the physiological response of Amazon forests, decreasing the availability to absorb atmospheric CO_2, as well as biodiversity and increasing risk of fires. Droughts on this region also affect population by isolating them due to anomalous low river levels. Impacts of droughts over NEB region are related to water and energy security and subsistence agriculture. Most drought episodes over Amazonia and NEB are associated with El Niño (EN) events, anomalous warming over the Tropical North Atlantic (TNA), and even an overlapping among them. However, not all the dry episodes showed a large-scale pattern linked to a canonical EN event or warm TNA episodes. For instance, dry episodes linked to EN events present distinct spatial patterns of precipitation anomalies depending on EN type (Central-Pacific vs. Eastern-Pacific EN), and NEB region experienced a severe drought in 2012 that is not attributed to EN or warm TNA events. Even in the case of the strong EN in 2015/16, some regional impacts have not been explained by EN contribution. This paper discusses the effects of CP and EP EN events, and the role of warm TNA events on tropical Walker and Hadley circulation leading to drought over Amazonia and NEB regions.

KEYWORDS

Amazonia, drought, ENSO, Northeast Brazil, precipitation, TNA

1 | INTRODUCTION

Together with global and regional warming, the last two decades have experienced three major droughts in the Amazon region (2005, 2010, 2016) and a large-scale drought affecting Northeast Brazil (NEB) since 2012 (Alvala *et al.*, 2019; Aragao *et al.*, 2018; Marengo *et al.*, 2018a; 2018b and references quoted in). This raises concerns about the resilience of tropical forests in the Amazon and semiarid biome in NEB to extreme droughts. The occurrence of these droughts leads to socio-economical impacts over these regions because drought conditions severely disrupt the livelihood of riverine, urban population, and the ecological functioning of the forest in the Amazon and the semiarid region population.

Earlier studies documented negative rainfall anomalies in Amazonia and NEB during El Niño (EN) (Ropelewski

and Halpert, 1987). In fact, El Niño-Southern Oscillation (ENSO) induces extreme droughts over Amazonia (e.g., 1912, 1925, 1983, 1987, 1998, 2010, 2016) and NEB (e.g., 1902, 1951, 1958, 1966, 1983, 1987, 1998, 2010, 2016). However, the drought conditions in Amazonia and NEB are also related to warm sea surface temperature (SST) anomalies over the Tropical North Atlantic (TNA) ("warm TNA event" hereinafter), or even the overlapping of both. The change of SST in the equatorial Pacific Ocean and North Atlantic Ocean inhibits precipitation over the equatorial Amazonia and thus induces droughts in various regions of Amazonia and semiarid lands of NEB (Andreoli *et al*., 2012; Jiménez-Muñoz *et al*., 2016).

While droughts occur in the semiarid lands of NEB, extreme droughts related to EN occur over the tropical forest of the Amazonia. Overall, these Amazonian droughts affect the north-central Amazonia, but the spatial pattern differs from one EN event to another and even from one drought year to another. Moreover, not all EN events produce extreme drought in Amazonia or NEB, as well as all droughts in Amazonia or NEB are not linked to EN (Marengo *et al*., 2008; Alvala *et al*., 2019). For instance, the non-EN drought in 2005 affected mostly southwestern Amazonia, while EN 2016 aggravated the dry conditions that started in 2012 (also a non-EN year) in NEB. Thus, each drought event is also different in duration, spatial coverage and intensity, as in the case of 2012, where droughts conditions prevailed in NEB while at the time record floods were detected in the Amazonia (Marengo *et al*., 2013).

Different patterns have been observed in the tropical Pacific SST anomalies during El Niño events and in the meridional SST gradient in the tropical Atlantic during drought years in Amazonia and NEB, and recent research suggests interactions and feedbacks between Tropical Pacific, TNA, and Indian Ocean (Cai *et al*., 2019). Previous studies documented the existence of different "types" of EN or EN flavours depending on the location of maximum warm anomalies over the tropical Pacific: Eastern Pacific (EP) EN or Central Pacific (CP) EN (Kao and Yu, 2009; Takahashi *et al*., 2011). Hadley and Walker circulations are differently affected during EP and CP EN episodes (Zheleznova and Gushchina, 2017), thus leading to different precipitation anomalies over South America (Hill *et al*., 2011; Tedeschi and Collins, 2015; Sulca *et al*., 2018).

Therefore, this study aims to explore the influence of the EP EN, CP EN, and warm TNA events in the regional distribution of the drought in Amazon and NEB. It is important to remark that the term 'drought' is used in this study in the sense of meteorological drought.

We will focus on the strongest episodes in 1983 (EP EN), 1998 (EP EN), 2005 (warm TNA), 2010 (CP EN + warm TNA), 2012 (non-EN and non-warm TNA), and 2016 (CP EN). As far as we know, previous studies did not analyse all these drought episodes together. This paper is organized as follows: Section 2 describes the climatic datasets and methods, in Section 3 we identify the major CP and EP EN types and events related to warm SST anomalies over the TNA, Section 4 includes the analysis of SST and precipitation anomalies, and Section 5 includes the analysis of atmospheric circulation anomalies observed during each event. Section 6 discusses the results obtained in this study, and it contains some concluding remarks.

2 | MATERIALS AND METHODS

2.1 | Datasets

The Climate Hazards Group InfraRed Precipitation with Stations (CHIRPS) version 2.0 was selected in this study to analyse the precipitation anomalies. CHIRPS dataset was developed by the USGS Earth Resources Observation and Science Center in collaboration with the Santa Barbara Climate Hazards Group (CHG) at the University of California. This dataset includes a quasi-global (50°S–50°N; 180°E–180°W) gridded precipitation time series from 1981 to present at 0.05° resolution (Funk *et al*., 2014). CHIRPS dataset was created for the monitoring of drought and trend analysis, and it is available freely at the CHG web portal http://chg.geog.ucsb.edu/data/chirps/. Selection of CHIRPS dataset among other existing datasets was based on previous studies evaluating the performance of this dataset over the tropics (Burton *et al*., 2018) and some regions of Brazil, including the NEB region (Paredes-Trejo *et al*., 2017; 2018; Nogueira *et al*. 2018).

Sea Surface Temperature (SST) fields were obtained from the European Centre for Medium-Range Weather Forecasts (ECMWF) latest atmospheric reanalysis ERA5 (Hirahara *et al*., 2016). This new reanalysis provides higher spatial and temporal resolutions and more recent model and data assimilation system than the previous ERA-interim reanalysis (Albergel *et al*., 2018). Monthly SST at 0.25° spatial resolution was used in this study.

EP and CP ENs were characterized by the C and E indices (Takahashi *et al*., 2011) provided by the Instituto Geofísico del Perú (IGP, www.met.igp.pob.pe/dataos/EC.txt). The advantage of C and E indices versus other indices such as those based on EN4 and EN3 regions is that C, E are poorly correlated, whereas EN3 and EN4 indices are autocorrelated (Takahashi *et al*., 2011). The oceanic index for characterization of SST anomalies over the TNA region was extracted from 'The state of the

ocean climate' initiative (http://sateteoftheocean.osmc.noaa.gov).

Wind and geopotential height anomalies at the low troposphere (850 hPa) were obtained from ERA-interim reanalysis (Dee *et al*., 2011). Divergence fields for latitudinal (10°N–30°S) and longitudinal (65–40°W) sections were obtained from NCEP/NCAR reanalysis (Kalnay *et al*., 1996).

2.2 | Methodology

Monthly values of both precipitation (CHIRPS) and SST (ERA5) datasets were used in this study, and they were averaged to produce seasonal values. We focus on this study on the analysis of austral summer (DJF) and autumn (MAM), and when appropriate, on the other seasons JJA and SON. Precipitation values were converted to mm·day^{-1}, even if they are provided for a given season. Anomalies were obtained by removing the average value for the reference period 1981–2010. Standardized anomalies were used in some cases, obtained from the ratio between the anomaly and the standard deviation of the reference mean.

The analysis of precipitation anomalies related to different EN or warm TNA events was performed from linear regression of seasonal precipitation anomalies onto the concurrent seasonal SST index (CP, EP, and TNA) such that

$$PP' = m \times SST'_{\text{index}} \tag{1}$$

where PP' is seasonal precipitation anomalies at each gridpoint, and SST'_{index} is the standardized seasonal SST index. Period 1981–2016 was used for this analysis. The coefficient m represents the strength of the seasonal climate responses that are associated with ENSO-related and TNA-related anomalous SSTs. The significance of the coefficients is tested using a Student's t test at the 95% confidence level.

Maps of residual (ε) precipitation anomalies (i.e., anomalies not related to any of the E, C, and TNA SST indices) were obtained by subtraction of predicted anomalies (PP'_{pre}) to the observed anomalies (PP'_{obs}):

$$\varepsilon = PP'_{\text{obs}} - PP'_{\text{pre}} \tag{2}$$

where PP'_{pre} is obtained from linear regression:

$$PP'_{\text{pre}} = a_1 \times SST'_{\text{E}} + a_2 \times SST'_{\text{C}} + a_3 \times SST'_{\text{TNA}} + a_0 \tag{3}$$

Trend analysis of precipitation and SST anomalies was performed for each grid point from Mann–Kendall analysis (Kendall, 1975) and Sen's method (Sen, 1968). These methods are nonparametric and make no assumptions on the distribution of data.

2.3 | Study area

The study area (Figure 1a) includes the Amazon forests and the Northeastern Brazil region. The Amazonian region includes about one-half of the world's tropical forests and is a key component of the global carbon cycle (Cox *et al*., 2000). Amazon forests were delimited using a land cover map (MODIS product MCD12C1; Strahler *et al*., 1999) and the 'Evergreen Broadleaf Forest' class, with an estimated ground area of around 5.8 million km^2. This area was divided into four different geographical regions to account for different seasonality, namely, Northwestern (NW), Northeastern (NE), Southwestern (SW), and Southeastern (SE) regions. NEB region was delimited from a geographical vector (shapefile), with a total ground area of 1.5 million km^2 (around 20% of the Brazilian territory). It is bordered by the Amazon forest (west), the Atlantic Ocean (east and north), and the states of Minas Gerais and Espírito Santo (south). The predominant climate y semiarid type. This feature makes the region an anomalous area when compared to the other areas in the same latitudinal range.

Seasonal precipitation patterns are markedly different between Amazonia and NEB, and also between different regions over Amazonia (Figure 1b). Roughly, the rainy season over Northern Amazonia occurs during the austral autumn/winter, whereas the dry season occurs during the austral spring/summer, and the pattern is approximately reversed over Southern Amazonia. NEB region shows regional variations, with a rainy season over Northern NEB during austral fall and over the coastal area of Eastern NEB during austral winter, and a widespread dry season over the semiarid region during austral spring. The amount of maximum precipitation over Amazonia is approximately four times greater than over NEB.

3 | IDENTIFICATION OF INTENSE WARM EP, CP, AND TNA EVENTS

We identified different intensities of warm EP, CP and TNA events based on thresholds applied to SST anomalies for E and C indices, and SST anomalies over the TNA region (Table 1). In the case of E and C indices, thresholds were applied to seasonal values for the period DJF. Intensities were categorized into 'weak', 'moderate', 'strong', and 'very strong' using threshold values of 0.5, 1.0, 1.5 and 2.0°C, respectively. In the case of TNA SST

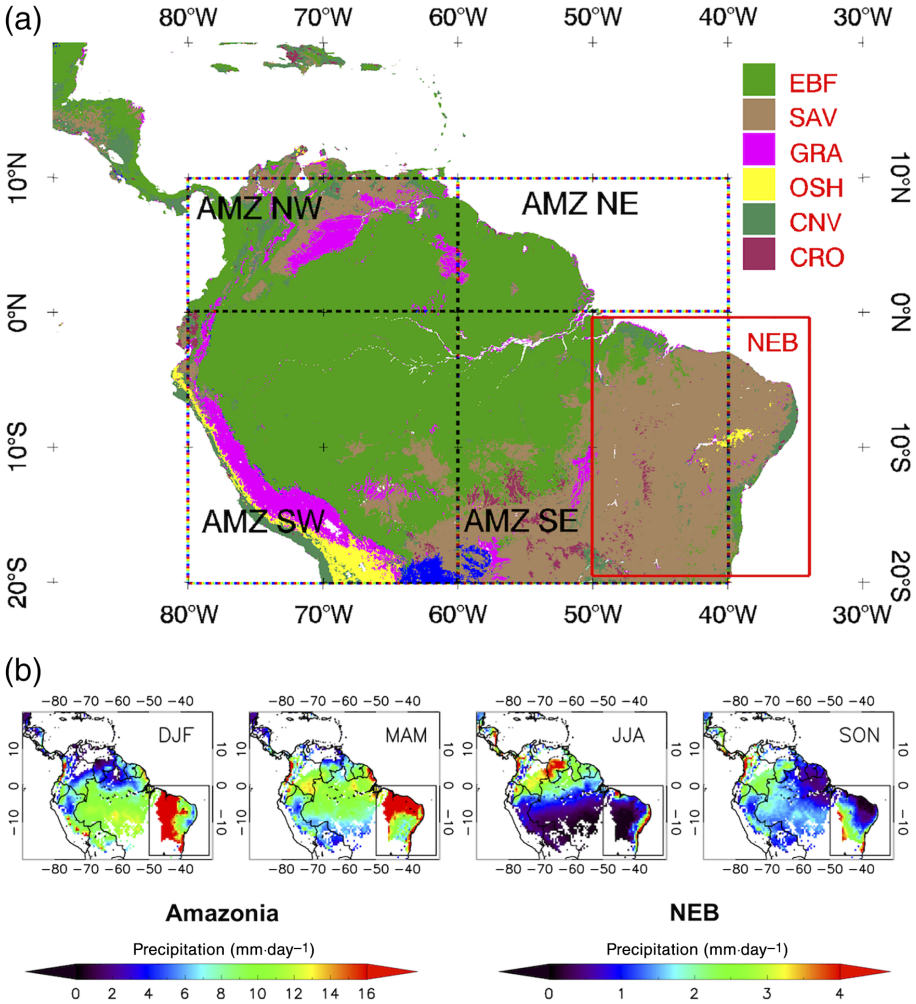

FIGURE 1 (a) Land cover maps of the study area (EBF: Evergreen Broadleaf Forest; SAV: Savanna; GRA: Grassland; OSH: Open Shrubland; CNV: Crop and natural vegetation; CRO: Cropland). Dashed boxes indicate the four Amazonian (AMZ) subregions (NW: Northwest, NE: Northeast, SW: Southwest, SE: Southeast). The box indicates the Northeastern Brazil (NEB) region. (b) Climatological mean values (1981–2010) of seasonal (DJF, MAM, JJA, SON) precipitation over the study area. Values are provided in mm·day^{-1}. Precipitation over NEB was rescaled for visualization purposes [Colour figure can be viewed at wileyonlinelibrary.com]

anomalies, thresholds were applied to seasonal values for the period MAM. Because the magnitude of the anomaly over the TNA is lower than the magnitude of the anomaly over the tropical Pacific, threshold values were reduced to 0.25, 0.5, 0.75, and 1.0 for 'weak', 'moderate', 'strong', and 'very strong' categories, respectively.

Figure 2 shows the temporal evolution of E, C and TNA SST indices, where the different intensity categories are marked. In terms of EP EN events, 1983 and 1998 were categorized as 'very strong', and 2016 as 'strong'. The most intense CP EN event in the last seven decades was identified in 2010 (the only 'very strong' event), closely followed by the recent 'strong' event in 2016. Other past 'strong' CP EN events were also identified in 1992, 1969, and 1958. The only 'very strong' warm TNA event was identified in 2010, with a 'strong' event in 2005, and other past 'strong' events in 1969 and 1958. It is remarkable that the number of CP EN events is higher than the number of EP EN events, although most of the CP EN events were categorized as 'weak' or 'moderate'. The number of warm TNA events was also higher than the number of EP EN events, with sustained warm anomalies almost from 1995 to present.

Spatial patterns of SST anomalies for the strongest warm events are illustrated in Figure 3. The three strongest EN events (1983, 1998, 2016) show high warm SST anomalies over the tropical Pacific peaking in DJF and partly sustained in MAM (although in 2016 positive SST anomalies are lower but extended over adjacent sea regions). In the case of 2016 EN, EP presented warm condition but was lower than in EN events 1983 and 1998, consistent with the categorization of EP EN for 1983 and 1998 and CP EN for 2016. In the case of 2010 EN

TABLE 1 Thresholds values selected for the categorization of different intensities for warm EP, CP, and TNA events

Category	E or C	TNA
Weak	$0.5 \leq SST' < 1.0$	$0.25 \leq SST' < 0.5$
Moderate	$1.0 \leq SST' < 1.5$	$0.5 \leq SST' < 0.75$
Strong	$1.5 \leq SST' < 2$	$0.75 \leq SST' < 1.0$
Very strong	$SST' \geq 2.0$	$SST' \geq 1.0$

Note: Values refer to sea surface temperature anomalies (SST′) in K.

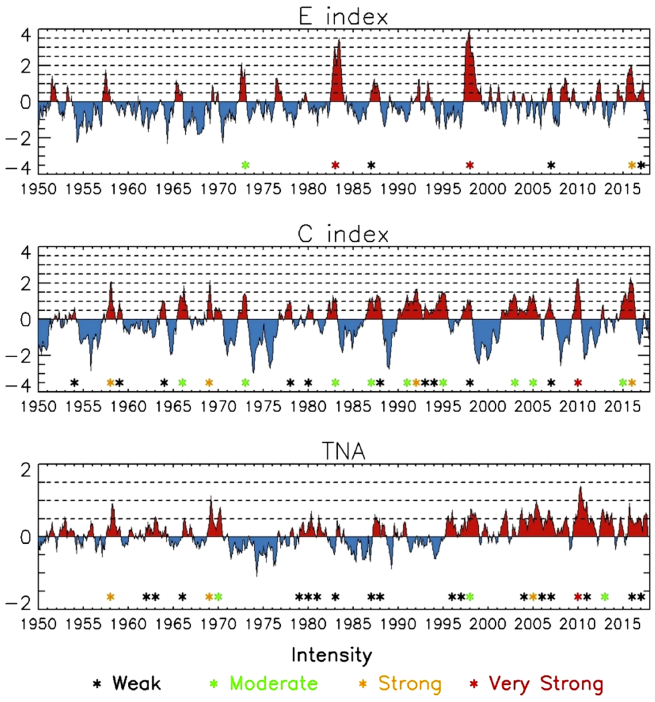

FIGURE 2 Temporal series of monthly values for E, C, and TNA SST indices. The different intensities of particular events were categorized into 'weak', 'moderate', 'strong', and 'very strong' depending on the seasonal value of positive SST anomalies (see Table 1). The asterisks indicate the year of each event [Colour figure can be viewed at wileyonlinelibrary.com]

conditions are also observed, with the strongest warming over the CP. The strongest warm SST anomalies over TNA are observed in 2005 and 2010 during the MAM season. Warm anomalies are also observed over the TNA region in MAM-1998, but almost neutral anomalies in MAM-1983 and MAM-2016.

During the austral winter (JJA) a transition to cold SST anomalies (La Niña conditions) is observed in all the three cases, with 1998 providing the coldest SST anomaly over EN regions, with a strong warm anomaly near the coast of Peru (EN1 + 2 region) in 1983, and 2016 evidencing a widespread warming over adjacent sea regions (Figure S1). Warm SST anomalies over TNA region were also partly sustained during JJA in 2005 and 2010.

4 | INFLUENCE OF SST ANOMALIES ON PRECIPITATION ANOMALIES OVER AMAZONIA AND NEB REGION

In this section we analyse the precipitation anomalies over Amazonia and NEB regions for the major EN and warm TNA events shown in the previous section, with attention to the impact of EP and CP ENs. We also focus on the identification of features or drought episodes that are not linked to EN or TNA events.

4.1 | Spatial patterns of precipitation anomalies during EN and warm TNA events

Figure 4 shows the spatial patterns of precipitation anomalies over Amazon forests and NEB region for the warm EP, CP, and TNA events presented in Figure 3. The three major EN events (1983, 1998, 2016) show widespread precipitation deficits over Amazonia during the austral summer (DJF), while vanishing during the austral autumn (MAM), except in the case of 1983 with an intense negative precipitation anomaly over eastern Amazonia.

In contrast, the two major warm TNA events (2005, 2010) show a characteristic north–south contrast during MAM, with wet conditions over northern Amazonia and dry conditions over southern Amazonia. In the case of 2010, widespread precipitation deficits are also observed over Amazonia, especially over northern Amazonia, which may be attributed to the occurrence of EN event previous to the warm TNA event in MAM.

In the case of the NEB region, the driest conditions are observed during the austral autumn. In the case of EN events (1983, 1998, 2016), widespread precipitation deficits are observed, whereas in the case of the warm TNA events in 2005 and 2010 the precipitation deficits focus on northern NEB. In contrast to observations over Amazonia, during the previous season (DJF) precipitation deficits are lower, although incipient dry conditions are also observed, especially over northern NEB.

During the austral winter (JJA), only weak precipitation deficits are observed over Amazonia (except for 1983 with still intense precipitation deficits over northeastern Amazonia), and almost neutral precipitation anomalies are observed over NEB (Figure S1). The other strong CP EN in 1992 shows widespread precipitation deficits over Amazonia in DJF and MAM and a transition from wet conditions over NEB in DJF to intense precipitation deficits in MAM. Precipitation deficits remained over northeastern Amazonia in JJA (Figure S2).

4.2 | Precipitation deficits linked to non-ENSO/non-warm TNA events

Precipitation deficits presented in the previous section occurred under warm SST anomalies over the tropical Pacific and/or North Atlantic. However, precipitation deficits are also observed under conditions not

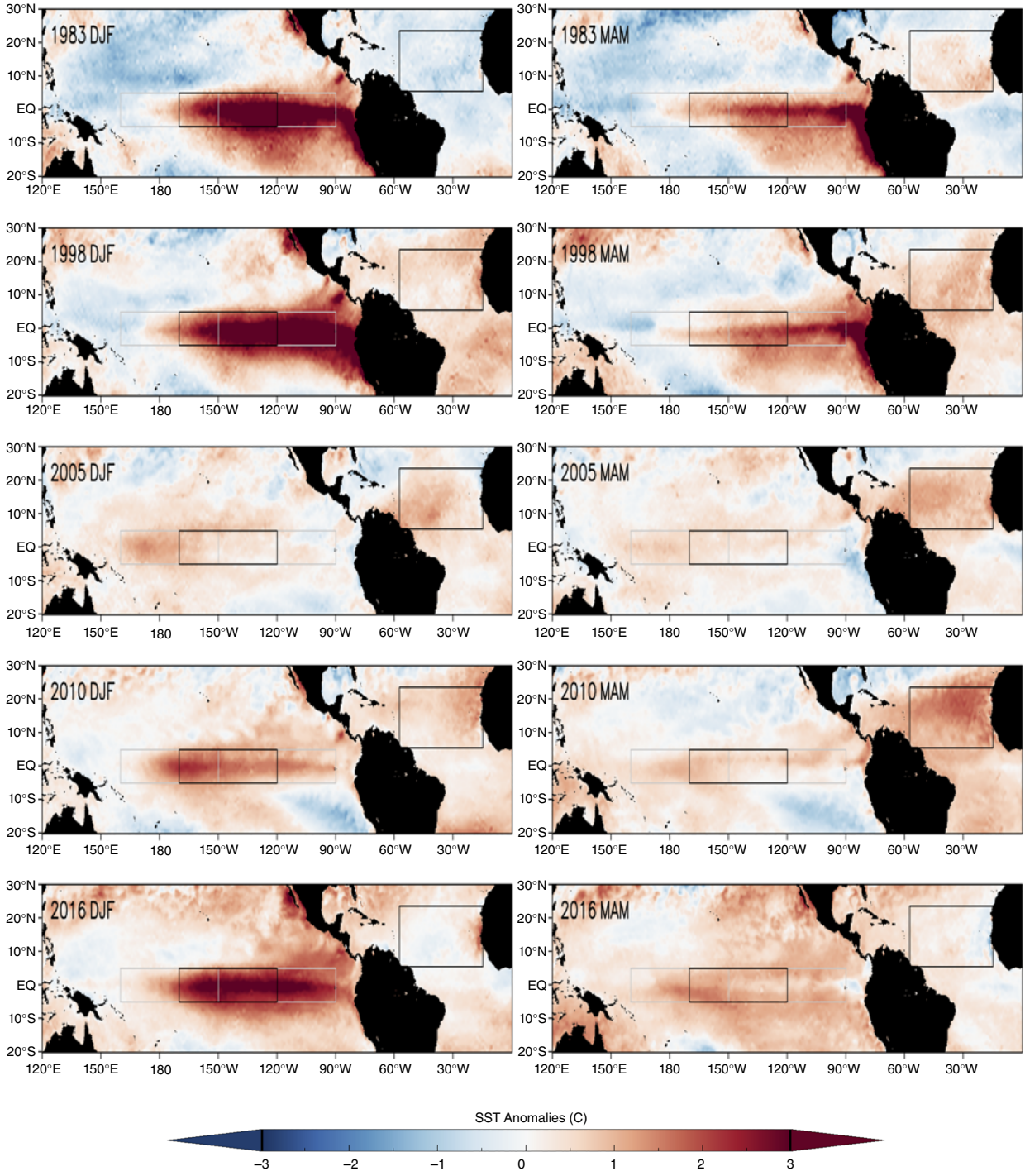

FIGURE 3 Spatial patterns of seasonal (DJF and MAM) sea surface temperature (SST) anomalies for different EP EN, CP EN, and warm TNA events (see Figure 2). The two grey boxes mark EN3 and EN4 region, and black boxes mark EN3.4 and TNA regions [Colour figure can be viewed at wileyonlinelibrary.com]

necessarily linked EN or warm TNA events, and in some cases these precipitation deficits occurred even under cold SST anomalies. Figure 5 shows scatter plots of precipitation (MAM season) and SST (DJF season) standardized anomalies (E, C, and TNA indices) over different Amazonian geographical sectors, and Figure 6 includes the scatter plots over the NEB region. Precipitation deficits under cold SST anomalies are represented by yellow circles, with significant dryness (standardized anomalies < -1) represented by filled circles. In the case of Amazonia (Figure 5), years 1985 and 1988 showed precipitation deficits under cold SST anomalies over some

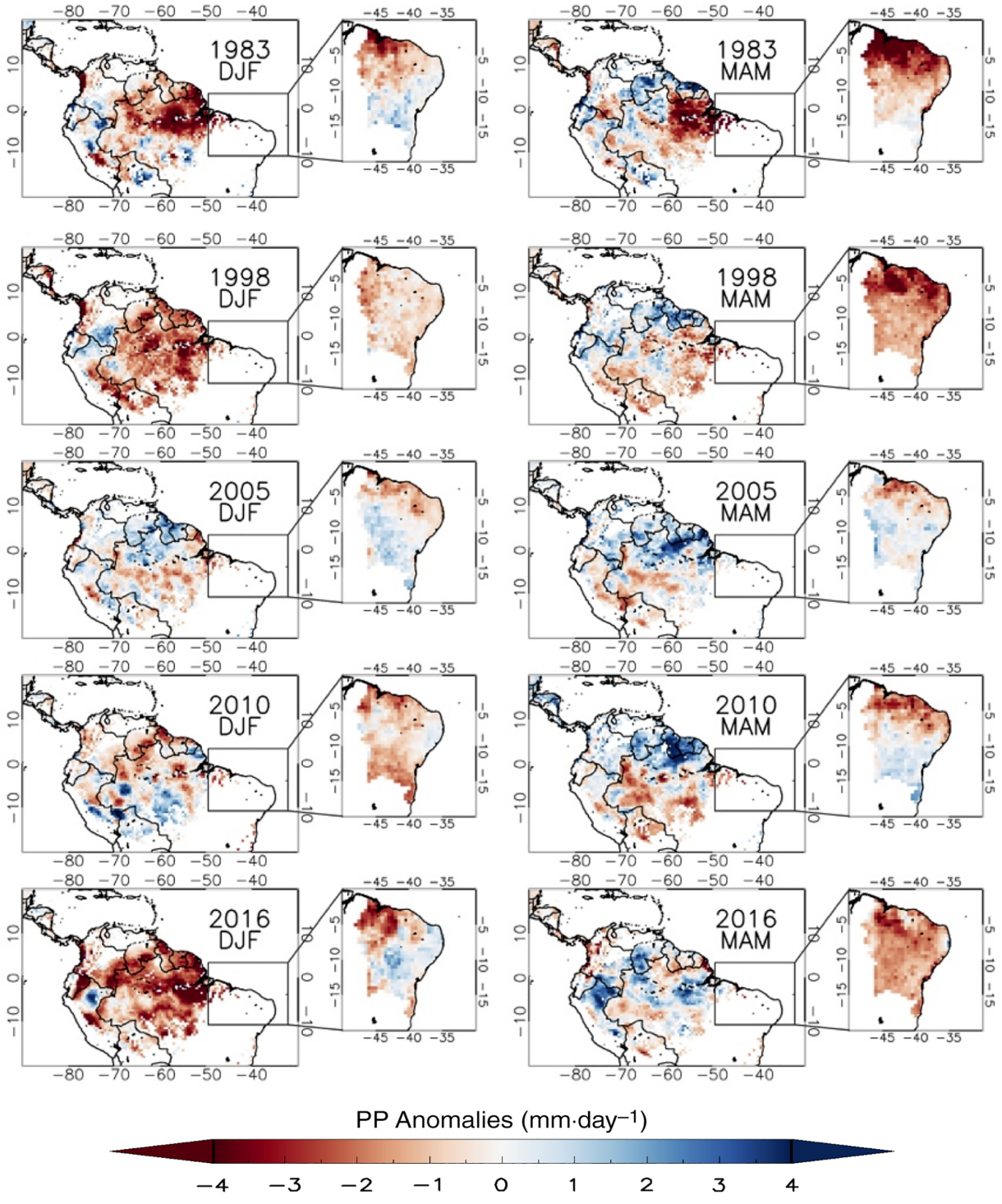

FIGURE 4 Spatial patterns of precipitation anomalies during seasons DJF, MAM, and JJA for different strong EN and TNA events. Values are only displayed over Amazon tropical forests and NEB region. The zoom over the NEB region is marked by a black box for a better visualization [Colour figure can be viewed at wileyonlinelibrary.com]

sea regions. Same occurred for the NE region in 1986, 1992, and 2009, and SW region in 1983 and 1992. The SW region did not experience any dry/cold event. NEB region (Figure 6) experienced dry/cold events in 1990, 1992, 1993, and 2012, with this last year providing the lowest precipitation anomaly in our study period.

Figure 7 shows the spatial patterns of SST and PP anomalies for 1990, 1993, 2012 (results for 1992 are provided in Figure S2). SST anomalies do not show any characteristic pattern over EN or TNA regions, more than slight warm anomalies over tropical Pacific in MAM-1993 or slight cold anomalies (La Niña conditions) in

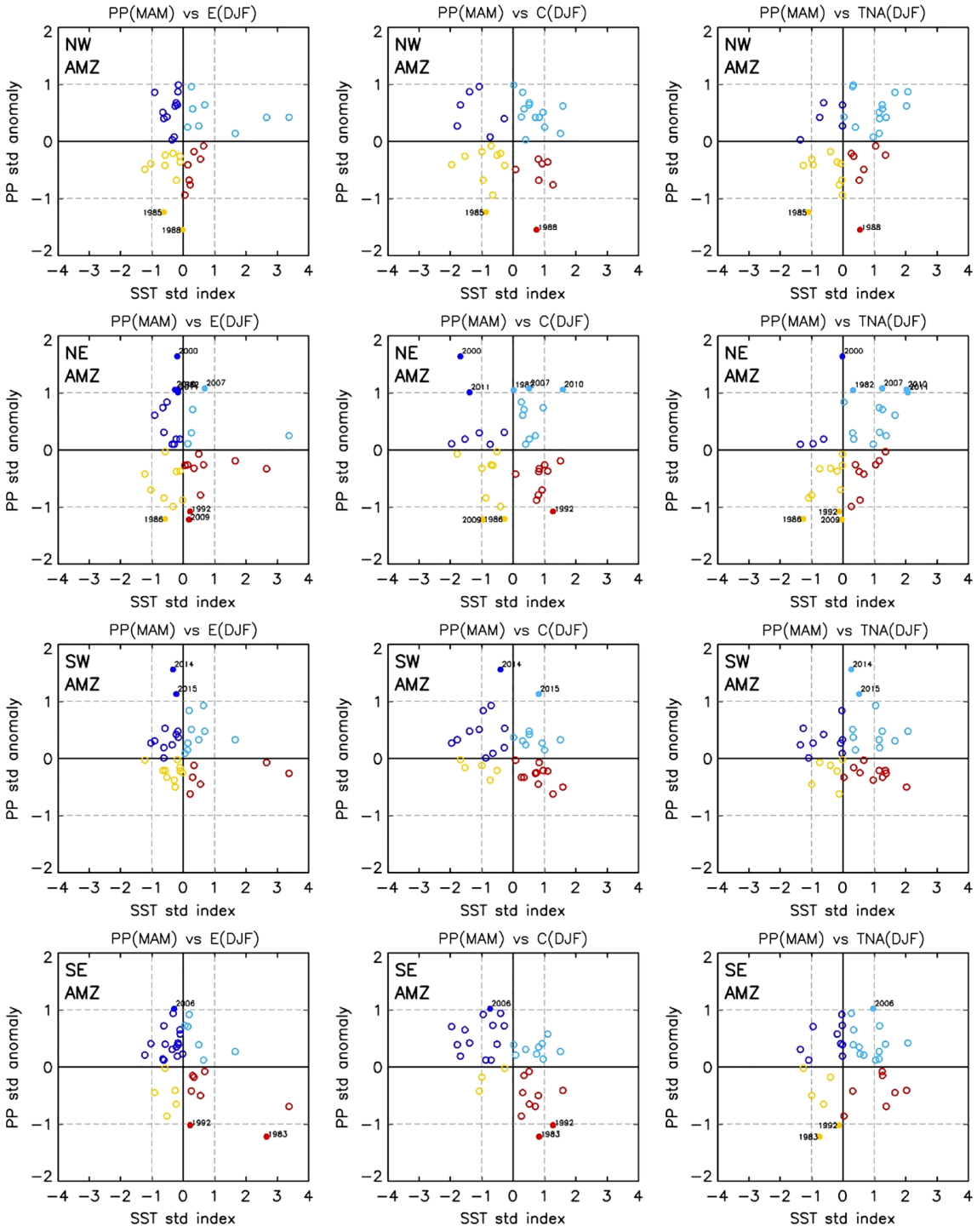

FIGURE 5 Scatter plots of standardized precipitation (PP) anomalies during the MAM season versus standardized sea surface temperature (SST) anomalies during the DJF season using three SST indices (E, C, TNA) and four regions over Amazonia (NW: Northwest, NE: Northeast, SW: Southwest, SE: Southeast). Dark blue circles indicate wet episodes under cold SST conditions, light blue circles indicate wet episodes under warm SST conditions, yellow circles indicate dry episodes under cold SST conditions, and red circles indicate dry episodes under warm SST condition. Filled circles were used for those cases where PP standardized anomalies exceeded one standard deviation [Colour figure can be viewed at wileyonlinelibrary.com]

DJF-2012. However, precipitation deficits were intense and widespread over NEB region during MAM, with incipient dry conditions also observed during DJF in 1993 and 2012 (in contrast to widespread wet conditions observed in DJF-1990). It is also remarkable the widespread wet conditions observed over Amazonia during these three events for the DJF season, especially in 2012.

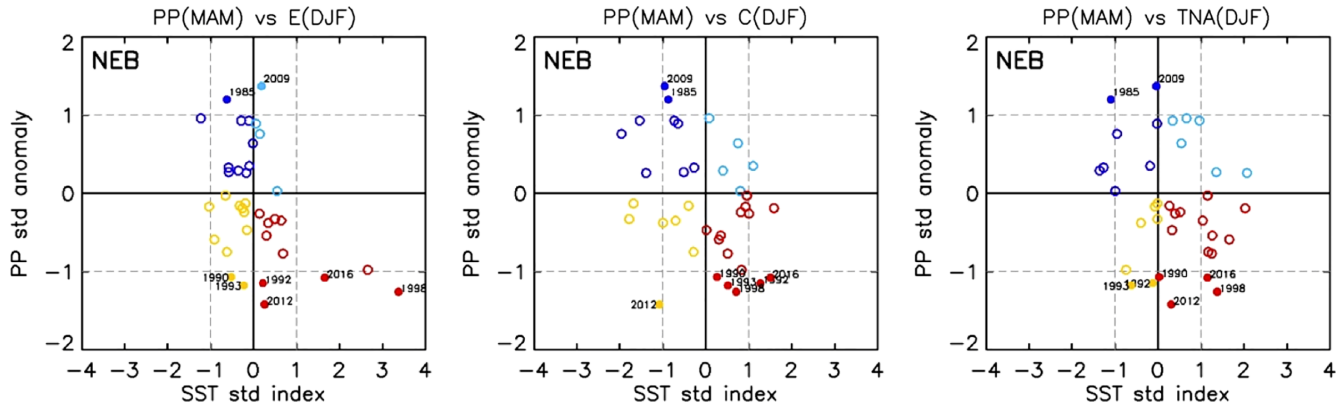

FIGURE 6 Same as Figure 5, for the Northeastern Brazil (NEB) region [Colour figure can be viewed at wileyonlinelibrary.com]

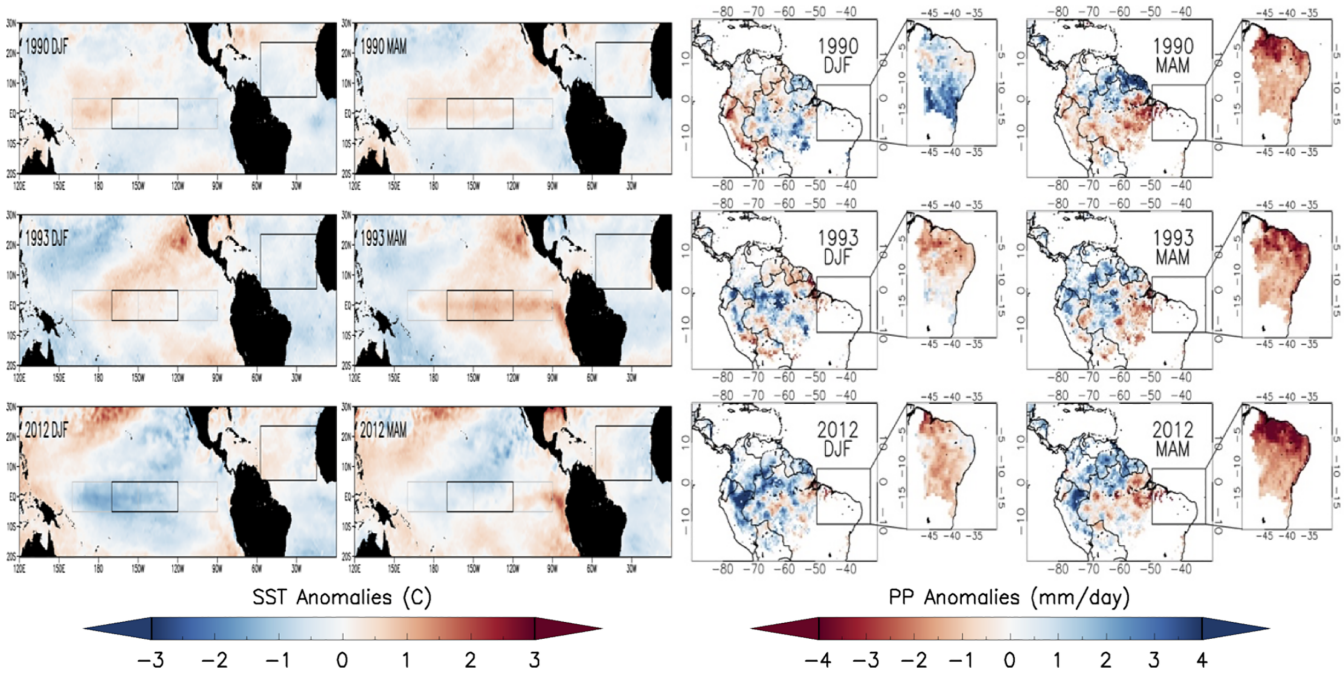

FIGURE 7 Spatial patterns of sea surface temperature (SST) (left) and precipitation (PP) (right) anomalies during DJF and MAM seasons for years 1990, 1993, and 2012. These years were not linked to EN neither warm TNA events, but they are linked to strong precipitation deficits over NEB region [Colour figure can be viewed at wileyonlinelibrary.com]

4.3 | Contribution of E, C, and TNA to observed precipitation anomalies

Linear regression analysis of precipitation anomalies at each gridpoint on area-averaged (E, C, and TNA) SST anomalies was performed to better understand the role of the different ENSO flavours (E vs. C) and TNA over the observed spatial patterns of drought in Amazonia and NEB. The slope of the regression is presented in Figure 8 for the three SST indices (E, C, TNA) and seasons DJF and MAM. During the austral summer, EN events inhibits precipitation over wide areas of Northeastern Amazonia, with a similar pattern for E and C indices. However, the signal of the C index is stronger than the signal of the E index. In the case of the NEB region the contribution of E and C is only significant over some regions of northern NEB, and again the signal for the C index is stronger than the E index.

During the austral autumn, the signal of E and C indices are weak over Amazonia, but they become strong over northern NEB, with E index providing a slightly higher signal than the C index. During this period, the signal of TNA over northern NEB is also significant and robust, whereas Amazonia shows a characteristic north–south dipole (wetness over northern Amazonia and dryness over southern Amazonia). During the austral winter

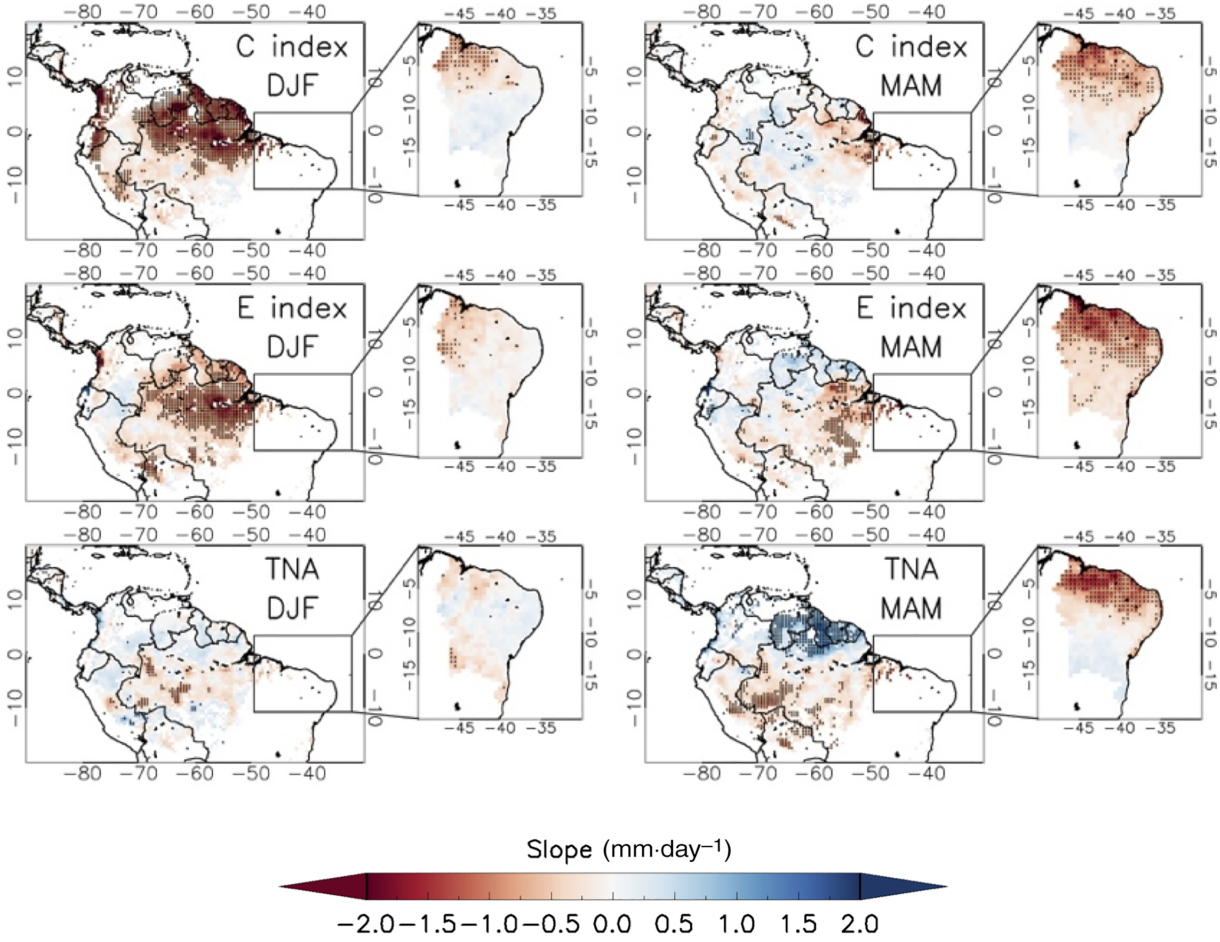

FIGURE 8 Linear regression coefficient between standardized SST indices (E, C, TNA) and precipitation anomalies for DJF and MAM seasons. Values are in mm·day^{-1} per standard deviation. Pixels at the 95% confidence level are marked [Colour figure can be viewed at wileyonlinelibrary.com]

the role of TNA is not significant, and only C and E indices show a weak signal. In this season the contribution of the E index is stronger than the C index, both over Amazonia and NEB (Figure S3).

The contribution of the different sea regions can also be analysed through the residuals, once the contribution from E, C, and TNA indices are removed from the actual precipitation anomalies (see Figure 4 for comparison). Results are presented in Figure 9. Overall, a wet pattern arises when E, C, and TNA contributions are removed, especially over Amazonia. However, in the case of 2012 over NEB, the dry pattern is similar to the actual precipitation anomalies (Figure 7), confirming a drought event not related to EN or a warm TNA event (weak La Niña conditions are observed during DJF-2012, Figure 7). It is also remarkable the dry conditions observed over some regions in DJF-2016, which are not explained by a linear contribution of EN or warm TNA conditions.

4.4 | Temporal trends

Time series of monthly precipitation are shown in Figure 10 over Amazonia and NEB regions. Rainfall deficits are observed over particular EN and warm TNA events, as presented in the previous sections, and it also shows a strong interannual variability of precipitation over these regions. A predominance of negative anomalies since 2012 is also observed over NE and NW Amazonia, and NEB. Spatial patterns of long-term (1980–2016) trends are presented in Figure 11, suggesting a significant wetting trend over northern Amazonia and a significant drying trend over NEB during the austral autumn, with a slight negative trend over southern Amazonia during this season. For the rest of seasons, the results are not conclusive, although a predominant drying trend is observed over Amazonia during the austral spring and over southern Amazonia and some regions of NEB during the austral summer.

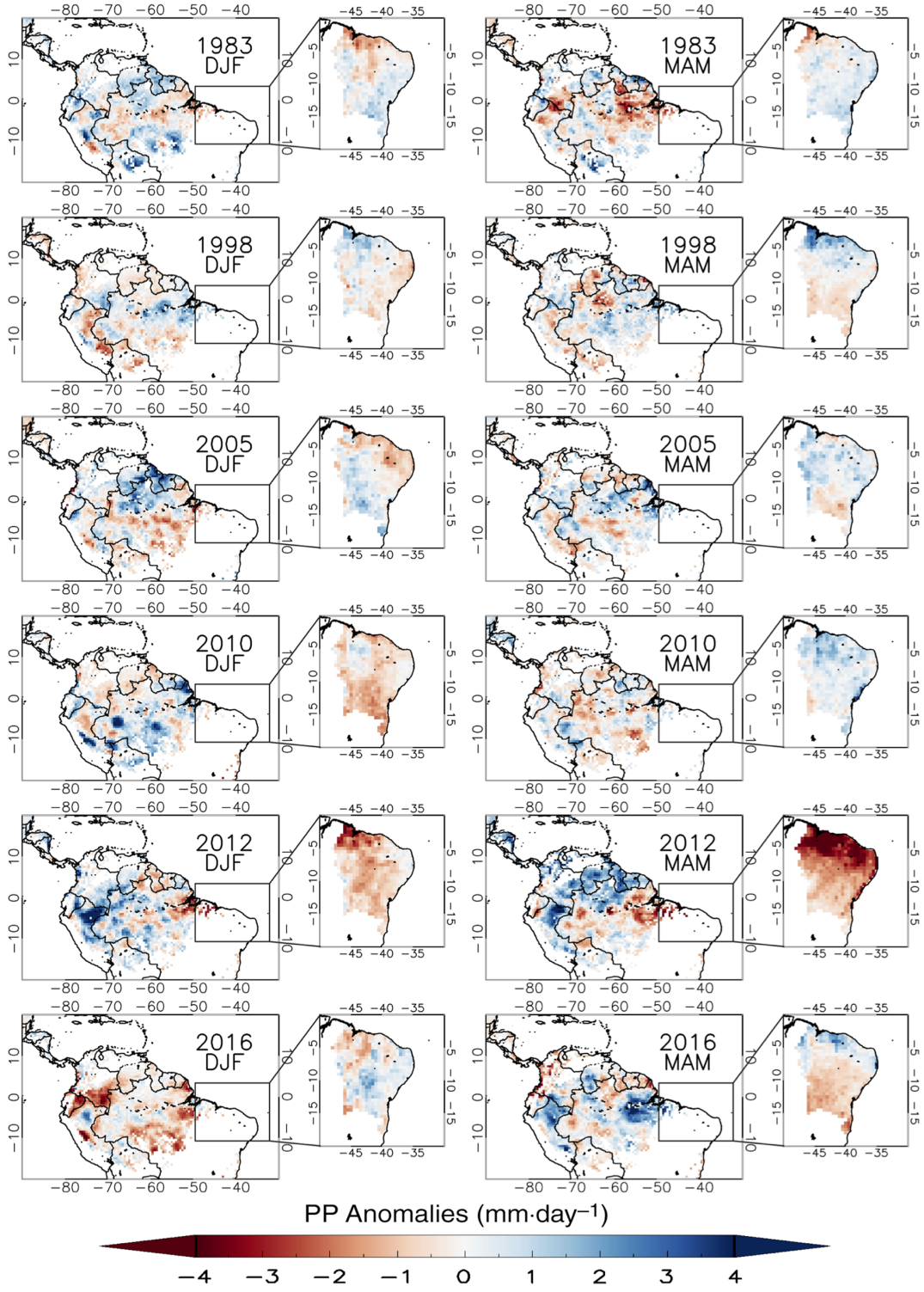

FIGURE 9 Residuals of precipitation anomalies after removal of contributions from E, C, and TNA indices [Colour figure can be viewed at wileyonlinelibrary.com]

In terms of trends of SST anomalies (Figure 12), EN regions show a slight warming trend but it is not significant. The TNA region shows a significant warming trend for austral spring and summer. A warming trend over TNA is also observed almost for all the seasons, and it is significant for the austral summer, winter, and spring, with this last season providing the highest value of the trend.

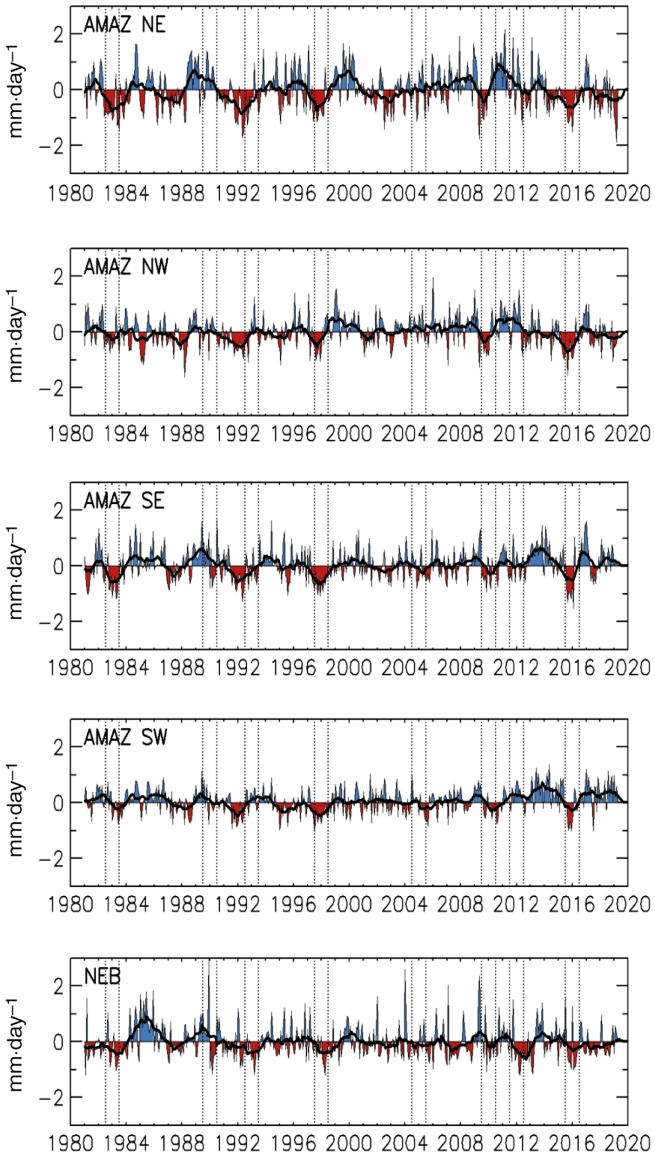

FIGURE 10 Temporal series of monthly precipitation anomalies (in mm·day^{-1}) over different Amazonian subregions and the NEB region. A 12-month running mean is overplotted [Colour figure can be viewed at wileyonlinelibrary.com]

5 | IMPACTS ON ATMOSPHERIC CIRCULATION

We discuss in this section the low-level circulation during austral summer (DJF) and autumn (MAM) based on wind anomalies at 850 hPa for the case studies of 1983, 1998, 2005, 2010, 2012, and 2016, as presented in Figure 13. The analysis is complemented through the zonal and meridional vertical velocity cross-sections over the Pacific, equatorial South America, and the Atlantic sectors that are shown in Figures 14 and 15, which at the same time provide information on the changes of the Walker's and Hadley circulations. This analysis should be considered in the context of the observed SST and rainfall anomalies for these events (Figures 3, 4 and 7 for the case of 2012).

Changes in large-scale circulation associated with SST patterns are responsible for rainfall anomalies, particularly during austral summer and autumn. In 1983, 1998, and 2016, all during strong EN events, changes in atmospheric circulation and rainfall were consistent with the notion of an active role of warmer-than-normal surface waters in 1983 over the equatorial Pacific during DJF and in the TNA in MAM, and in both DJF and MAM in 1998 and 2016 (Figure 3). Low-level atmospheric circulation anomalies in the Amazon and NEB regions show weakened northeast trades into tropical South America (Figure 13), determining less rainfall and drought conditions in both regions (Figure 4).

In 2005, the causes of the drought were not related to EN but an anomalously warm TNA, and near-surface circulation and moisture transport from the tropical Atlantic into southwestern Amazonia was reduced during the onset (DJF) and peak (MAM) of the summertime rainy season (Figure 13).

The trade winds over the tropical Pacific were weakened in 2010 consistent with EN conditions. Anomalously warm TNA mainly in MAM determined weakened Northeast trades over this sea region. The ITCZ was located anomalously northward displaced of its climatic position, by about 5° over equatorial Amazonia. At 10°S there is a strong flow from the Northeast coming from an intensified and northward displaced subtropical Atlantic high.

In 2012, there was a unique situation since both the Amazon and NEB showed contrasting rainfall patterns. The Atlantic moisture enters into the western part of Amazonia then turning southward to the southern Amazonia region, where the Chaco low was intensified. This latter was favoured by the intensification of subtropical high pressure over the region, associated with an anomalously intense and northward-displaced Atlantic high over a relatively colder subtropical South Atlantic Ocean (Marengo *et al.*, 2013). This pattern observed in 2012 was not found during other wet years in Amazonia such as 1989, 1999, and 2009. This suggests La Niña as the leading cause of the abundant rainfall in western Amazonia from October to December, with wet conditions starting earlier and remaining until March 2012, mostly in northwestern Amazonia. In NEB, the dry conditions started to appear in December 2011 in the northern sector and then extended to the entire region by the peak of the rainy season of February–May 2012, with the Northeast trades weakened during austral summer and suggesting an anomalously northward-displaced ITCZ.

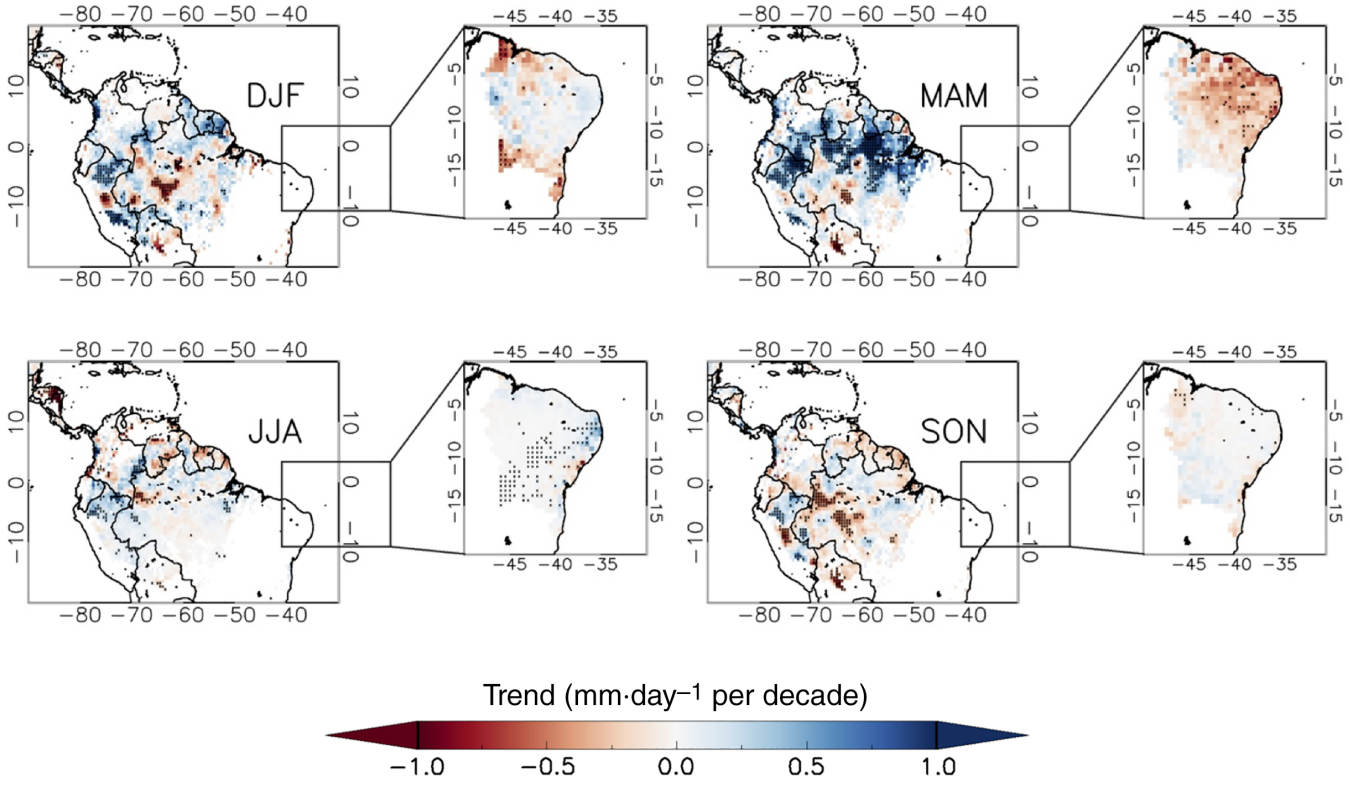

FIGURE 11 Trends in seasonal (DJF, MAM, JJA, SON) precipitation anomalies for the period 1981–2016. Pixels with values at the 95% confidence level are marked [Colour figure can be viewed at wileyonlinelibrary.com]

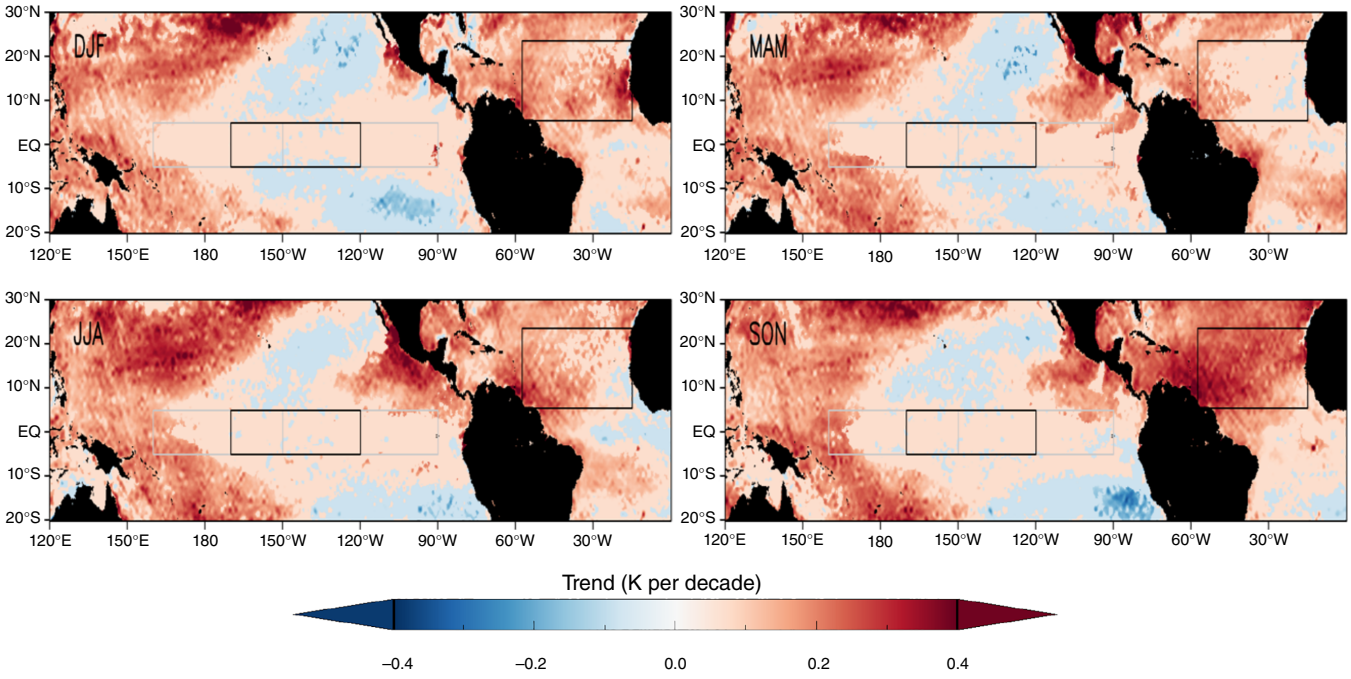

FIGURE 12 Trends in seasonal (DJF, MAM, JJA, SON) precipitation anomalies for the period 1981–2016. The graded colour scale is applied to pixels with values at the 95% confidence level. Light red (blue) colours are applied to pixels with positive (negative) nonsignificant values of the trend [Colour figure can be viewed at wileyonlinelibrary.com]

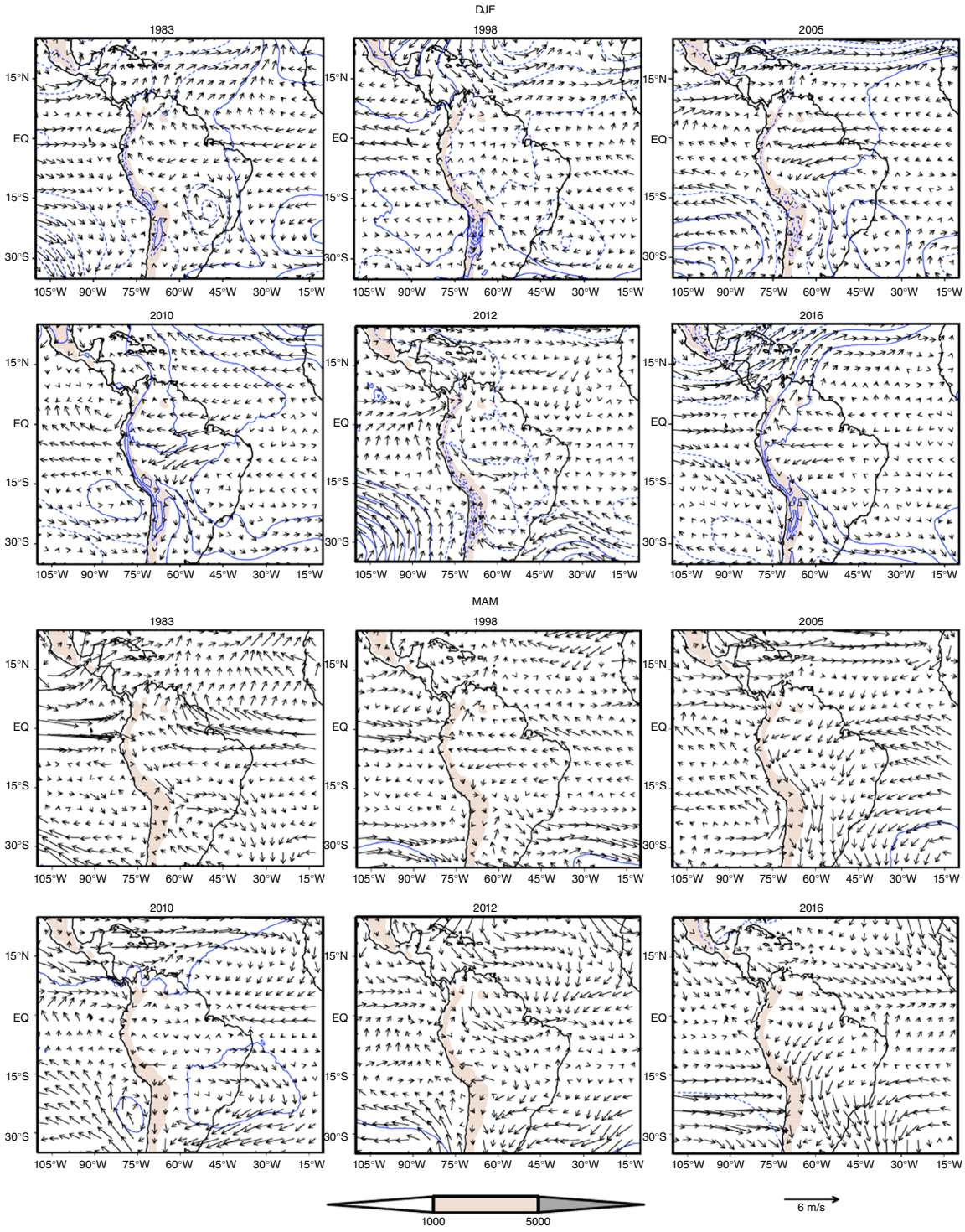

FIGURE 13 Anomalies of wind ($m \cdot s^{-1}$) and geopotential height (m) anomalies at 850 hPa for austral summer (DJF) and spring (MAM) during Amazonian droughts in 1983, 1998, 2005, 2010, 2012, and 2016. Solid (dot) blue lines represent anomalies of geopotential height in intervals of 50 m (−50 m). Brown shading represent topography of tropical Andes [Colour figure can be viewed at wileyonlinelibrary.com]

Anomalies for the zonal (Figure 14) and meridional (Figure 15) vertical circulation cross-sections are consistent with surface wind anomalies and with SST anomalies. Subsidence anomalies appear over areas with negative rainfall anomalies over Amazonia and NEB during drought and EN years, with convection and intense rainfall over warm SST in the eastern Pacific region. Upper-level convergence anomalies over the tropical

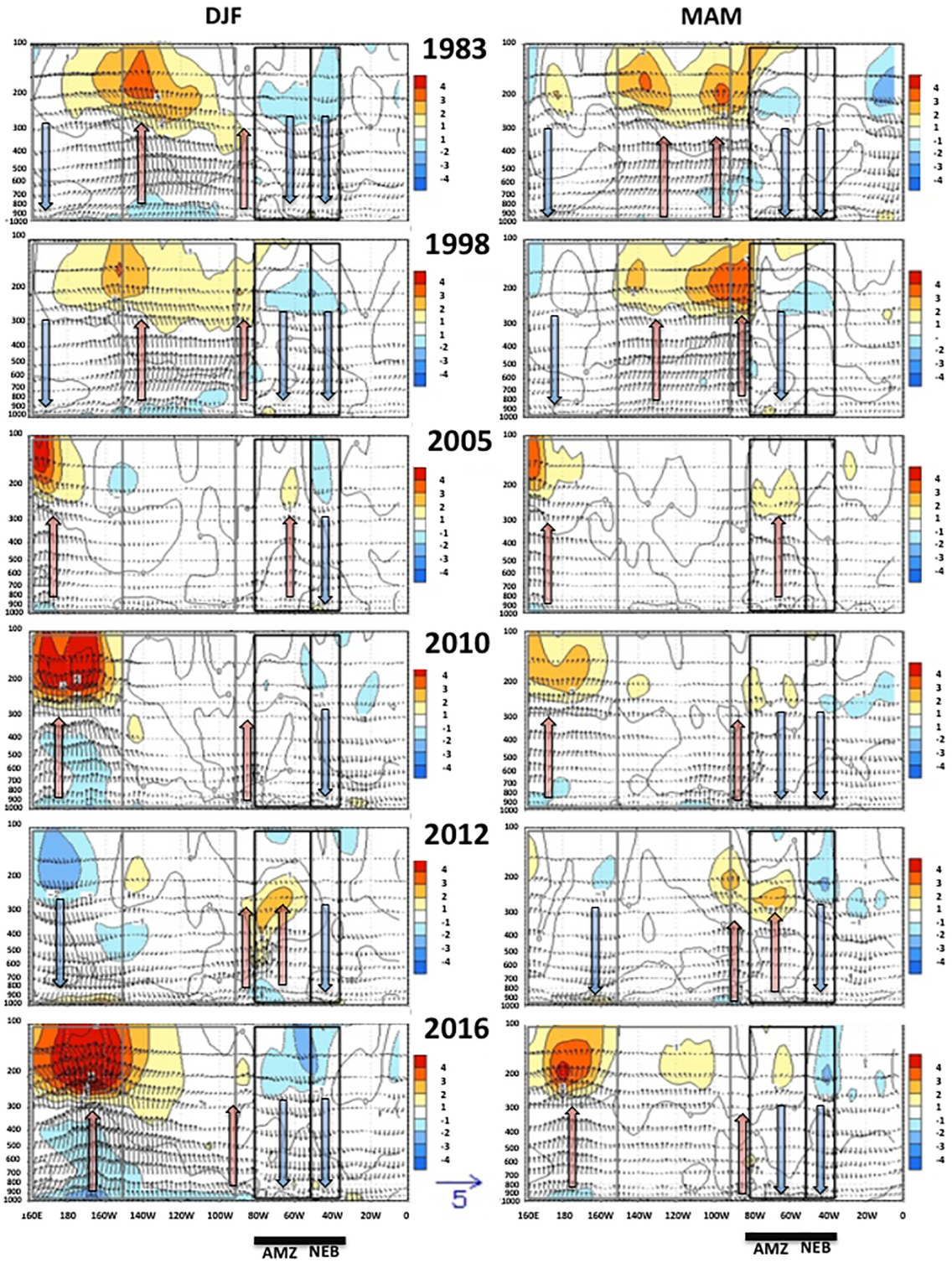

FIGURE 14 Pressure-longitude section (0–160°E) of the anomalous fields of divergence (contour interval is 10^{-6}·s^{-1}) and divergence, averaged between 5°N and 5°S. The divergent circulation is represented by vectors of combined pressure vertical velocity and the divergent component of the zonal wind. Red shading and solid contours denote divergence (left) and anomalous divergence (right). Blue shading and dashed contours denote convergence (left) and anomalous convergence (right). Anomalies are departures from the 1981 to 2010 base period seasonal means. Grey boxes delimitate EN4 and EN3 regions, and black boxes delimitate Amazonia (AMZ) and NEB regions. Red (blue) arrows indicate convection (subsidence) [Colour figure can be viewed at wileyonlinelibrary.com]

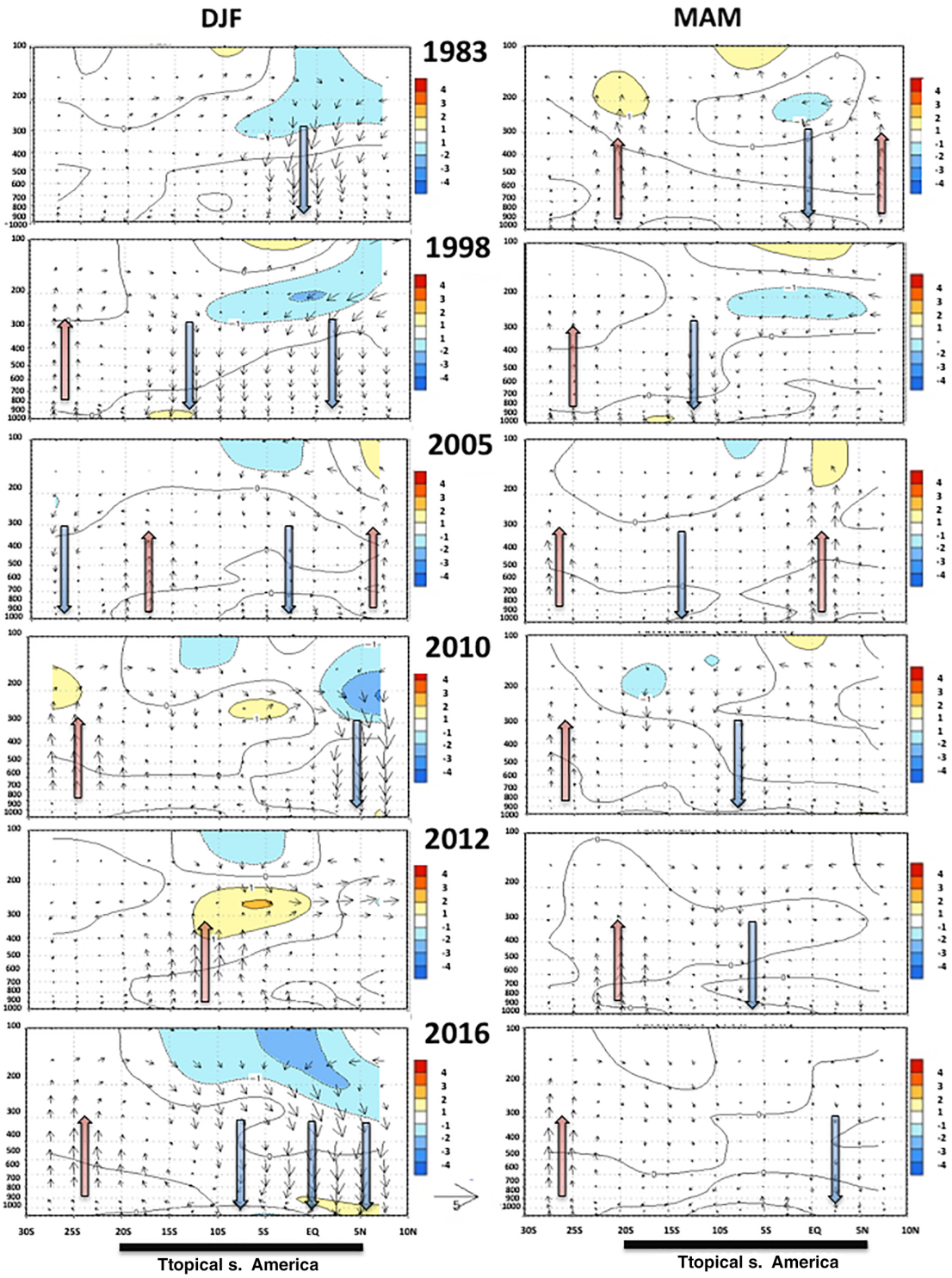

FIGURE 15 Pressure-latitude section (10°N–30°S) of the anomalous divergence (contour interval is $10^{-6}{\cdot}s^{-1}$) and divergence, averaged between 65 and 40°W. the divergent circulation is represented by vectors of combined pressure vertical velocity and the divergent component of the zonal wind. Red shading and solid contours denote divergence (left) and anomalous divergence (right). Blue shading and dashed contours denote convergence (left) and anomalous convergence (right). Anomalies are departures from the 1981 to 2010 base period seasonal means. Black boxes delimitate southern Amazonia (including NEB) and northern Amazonia. Red (blue) arrows indicate convection (subsidence) [Colour figure can be viewed at wileyonlinelibrary.com]

equatorial South America east of the Andes during drought years are consistent with low-level subsidence anomalies. Convection anomalies over oceanic areas with warm SST anomalies in the equatorial Pacific and compensatory subsidence over tropical South America are consistent with more or less rainfall in Amazonia and NEB. In 1983, 1998, 2010, and 2015 subsidence anomalies are observed over Amazonia, whereas in 2012 convection is detected over Amazonia and subsidence in NEB, consistent with rainfall anomalies in that year. This suggests anomalies in the upper and lower branches of the Hadley circulation over tropical South America east of the Andes, and of the Walker circulation over the equatorial Atlantic. Details on mean atmospheric circulation are included in Figures S4 and S5.

6 | DISCUSSION AND CONCLUSIONS

The impacts of droughts on Amazon and NEB climate and ecosystems can be markedly different because of the nature and location of warming in the tropical Pacific and Atlantic oceans and the location of the drought conditions across these regions. In the case of warming in the tropical Pacific, different impacts are also observed when warming is detected in the CP or the EP.

Spatial patterns of drought over the Amazon region during 1982–83, 1997–98, and 2015–16 were consistent with strong warming over the tropical Pacific during the austral summer DJF and to a lesser extent during the next season MAM, but with different intensities and patterns between these three events. Warming during the DJF season in 1982–83 and 1997–98 was strong in both CP and EP regions, while during the MAM season the warming was more intense in the EP region. Although the recent 2015–16 EN event was considered as strong as 1997–98 in terms of SST anomalies (L'Heureux *et al*., 2017), it was characterized by strong warming in the CP region and warmest air temperatures over Amazonia in 2016 (Marengo *et al*., 2018b), probably the highest temperature in a century (Jiménez-Muñoz *et al*., 2016). 2010 and 2016 are considered the strongest CP ENs in the last decades (with 1992 also showing a strong CP contribution; Figure 2). Droughts conditions were also evidenced over the NEB region during the three EN events in 1982–83, 1997–98, and 2015–16, particularly during the wet season MAM. This region was also affected by drought in MAM 2005 and 2010, linked to anomalous warming over the TNA region. However, in these last two cases droughts over NEB was focused over Northern NEB.

Correlation analysis between C, E, and TNA SST indices and precipitation anomalies indicated a strong signal of C and E over Amazonia during DJF, with a stronger signal for the C index than for the E index during this season (Figure 8). This result agrees with previous studies (Sulca *et al*., 2018). C and E indices are also indicative of rainfall deficits over NEB during the MAM season, with E index showing a slightly strongest signal than the C index. The role of TNA becomes significant mainly during the MAM season, with impacts in terms of rainfall deficits over southern Amazonia and northern NEB. It is particularly remarkable the widespread drought over NEB in 2012 and prevailing wet conditions over Amazonia, when cold surface water was detected in EP and CP and almost near normal SST anomalies in TNA. Extreme rainfall in Amazonia created a compensatory subsidence pattern in NEB that inhibited rainfall over that region in MAM (Marengo *et al*., 2013). Analysis of residual precipitation anomalies not linked to EN or warm TNA events (Figure 9) confirmed this result in 2012. Some regional rainfall deficits were also observed in the residuals for the EN event in 2016, indicating that warm SST anomalies over the tropical Pacific and TNA do not account for a complete description of the severity of the 2016 drought, as also reported also by Erfanian *et al*. (2017).

Time evolution of monthly precipitation shows a strong interannual variability, with a predominance of negative anomalies during the last decade over NE and NW Amazonia and NEB. Trend analysis during the austral summer evidences a contrasted pattern between northern (wet) and southern Amazonia/NEB (dry). However, a significant dry trend is hardly observed over the Peruvian Amazon, in contrast to the negative trend in river discharge from the 70s as suggested by Espinoza *et al*. (2011). Further analysis is required to assess to what extent this discrepancy is drawback of the CHIRPS dataset over the Andes or regions nearby. Trends of SST anomalies evidence a nonsignificant warming trend over the tropical Pacific, and a significant warming trend over TNA, especially during the SON and DJF seasons.

Physical mechanisms behind the different patterns of rainfall deficits during CP and EP ENs and warm TNA events can be described through the analysis of zonal and meridional vertical circulation cross-sections together with low-level wind anomalies (Figures 13–15; Figures S4–S5). This analysis is indicative of anomalous behaviour of Walker and Hadley cells. Convection over the tropical Pacific is observed over the region with highest SST anomalies, and differences between EP EN (1993, 1998) and CP EN (2010, 2016) are observed in the zonal cross-sections (Figure 14 and Figure S4). Enhancement of subsidence is also consistent with rainfall deficits observed over different regions, in line with other studies aimed at the analysis of distinct ENSO flavours (Johnson and Kosaka, 2016; Sulca *et al*., 2018; Gu and Adler, 2019).

Despite the advances in the understanding of the ENSO phenomenon, its complexity jeopardizes a correct description by models during seasons where teleconnections are relatively weak (Tedeschi and Collins, 2015; Timmermans *et al*., 2018).

We finish up this discussion with some comments on impacts of drought over tropical forests, and particularly over Amazonia. Description of these impacts has been documented in detail over the last years because of the increased availability of ground-based measurements, modelled data and satellite data. Droughts have an essential role in reducing carbon uptake by tropical forests through a decrease in photosynthesis, an increase in tree mortality, and increasing autotrophic respiration, as well as favouring the occurrence of wildfires (Brando *et al*., 2019). Fire incidence increased by 36% during the 2015–16 drought over Amazonia compared to the preceding 12 years, with fire locations outside the Arc of Deforestation (Aragao *et al*., 2018) and differences in the carbon releases by the fires around 2.4 PgC (Gloor *et al*., 2018). Furthermore, Malhi *et al*. (2018) showed this event led to a record rate of rising of atmospheric CO_2 of 3.4 ppm in 2016, resulting in the mean global atmospheric CO_2 concentration staying above the symbolically significant value of 400 ppm for the entire year. One-quarter of this record rise was caused by the biosphere's response to the impacts of EN fires in 2015–16 (the rest was from direct anthropogenic emissions). The tropical biosphere was a key element in the reduction of the global land carbon sink observed during this EN event (Liu *et al*., 2017), with some studies suggesting a reduction on photosynthesis in late 2015 and an increase in respiration during early 2016 (Luo *et al*., 2018). In particular, widespread reduction in sun-induced fluorescence over Amazon forests were observed during the 2015–16 El Niño, especially over the eastern part of the Amazon basin (Koren *et al*., 2018). These findings agree with the extreme drought observed over eastern/northeastern Amazonia during this period (Aragao *et al*., 2018; Jimenez *et al*., 2018).

In Northeast Brazil, the EN in 2015–16 increased the effect of the drought that started in 2010. Because of losses in the agricultural, cattle ranching, water supply and local economies due to the drought, the federal government authorized the release of resources for the affected districts to mitigate these negative impacts (Marengo *et al*., 2018a). According to the Ministry of Integration (www.mi.gov.br), during 2012–2016, 33.4 million people were affected by the drought, with estimated damage of R$ 104 billion (about US $ 30.0 billion).

All these impacts highlight the importance of a better understanding of mechanisms behind drought and their link to SST anomalies over sensitive sea regions for a better prediction and mitigation of these events.

ACKNOWLEDGEMENTS

This work was supported by the National Institute of Science and Technology for Climate Change Phase 2 under CNPq Grant 465501/2014-1, FAPESP Grant 2014/50848-9, the National Coordination for High-Level Education and Training (CAPES) Grant 16/2014.

ORCID

Juan C. Jimenez https://orcid.org/0000-0001-7562-4895
Juan C. Sulca https://orcid.org/0000-0003-4393-3161

REFERENCES

Albergel, C., Dutra, E., Munier, S., Calvet, J.-C., Munoz-Sabater, J., de Rosnay, P. and Balsamo, G. (2018) ERA-5 and ERA-interim driven ISBA land surface model simulations: which one performs better? *Hydrology and Earth System Sciences*, 22, 3515–3532. https://doi.org/10.5194/hess-22-3515-2018.

Alvala, R.C.S., Cunha, A.P., Brito, S.S.B., Seluchi, M.E., Marengo, J. A., Moraes, O.L.L. and Carvalho, M.A. (2019) Drought monitoring in the Brazilian semiarid region. *Annals of the Brazilian Academy of Sciences*, 91, e20170209. https://dx.doi.org/10.1590/0001-3765201720170209.

Andreoli, R., De Souza, F., Kayano, M.T. and Candido, L.A. (2012) Seasonal anomalous rainfall in the central and eastern Amazon and associated anomalous oceanic and atmospheric patterns. *International Journal of Climatology*, 32(8), 1193–1205.

Aragao, L.E.O.C., Anderson, L.O., Fonseca, M.G., Rosan, T.M., Vedovato, L.B., Wagner, F.H., Silva, C.V.J., Silva Junior, C.H.L., Arai, E., Aguiar, A.P., Barlow, J., Berenguer, E., Deeter, M.N., Domingues, L.G., Gatti, L., Gloor, M., Malhi, Y., Marengo, J.A., Miller, J.B., Phillips, O.L. and Saatchi, S. (2018) 21st century drought-related fires counteract the decline of Amazon deforestation carbon emissions. *Nature Communications*, 9, 536. https://doi.org/10.1038/s41467-017-02771-y.

Burton, C., Rifai, S. and Malhi, Y. (2018) Inter-comparison and assessment of gridded climate products over tropical forests during the 2015/2016 El Niño. *Philosophical Transactions of the Royal Society B*, 373, 20170406. https://doi.org/10.1098/rstb.2017.0406.

Brando, P.M., Paolucci, L., Ummenhofer, C.C., Ordway, E.M., Hartmann, H., Cattau, M.E., Rattis, L., Medjibe, V., Coe, M. T. and Balch, J. (2019) Droughts, wildfires, and carbon cycling: a pantropical synthesis. *Annual Review of Earth and Planetary Science*, 47, 555–581. https://doi.org/10.1146/annurev-earth-082517-010235.

Cai, W., Wu, L., Lengaigne, M., Li, T., McGregor, S., Kug, J.-S., Yu, J.Y., Stuecker, M.F., Santoso, A., Li, X.C., Ham, Y.G., Chikamoto, Y., Ng, B., McPhaden, M.J., Du, Y., Dommenget, D., Jia, F., Kajtar, J.B., Keenlyside, N., Lin, X.P., Luo, J.J., Martin-Rey, M., Ruprich-Robert, Y., Wang, G.J., Xie, S.P., Yang, Y., Kang, S.M., Choi, J.Y., Gan, B.L., Kim, G.I., Kim, C.E., Kim, S., Kim, J.H. and Chang P. (2019) Pantropical climate interactions. *Science*, 363, 944.

Cox, P.M., Betts, R.A., Jones, C.D., Spall, S.A. and Totterdell, I.J. (2000) Acceleration of global warming due to carbon-cycle feedbacks in a coupled climate model. *Nature*, 393, 249–252.

Dee, D.P., Uppala, S.M., Simmons, A.J., Berrisford, P., Poli, P., Kobayashi, S., Andrae, U., Balmaseda, M.A., Balsamo, G., Bauer, P., Bechtold, P., Beljaars, A.C.M., van de Berg, L., Bidlot, J., Bormann, N., Delsol, C., Dragani, R., Fuentes, M., Geer, A.J., Haimberger, L., Healy, S.B., Hersbach, H., Hólm, E. V., Isaksen, L., Kållberg, P., Köhler, M., Matricardi, M., McNally, A.P., Monge-Sanz, B.M., Morcrette, J.-J., Park, B.-K., Peubey, C., de Rosnay, P., Tavolato, C., Thépaut, J.-N. and Vitart, F. (2011) The ERA-interim reanalysis: configuration and performance of the data assimilation system. *Quaterly Journal of the Royal Meteorological Society*, 137, 553–597.

Erfanian, A., Wang, G. and Fomenko, L. (2017) Unprecedented drought over tropical South America in 2016: significantly under-predicted by tropical SST. *Scientific Reports*, 7, 581. https://doi.org/10.1038/s41598-017-05373-2.

Espinoza, J.C., Ronchail, J., Guyot, J.L., Junquas, C., Vauchel, P., Lavado, W., Drapeau, G. and Pombosa, R. (2011) Climate variability and extreme drought in the upper Solimoes River (western Amazon Basin): understanding the exceptional 2010 drought. *Geophysical Research Letters*, 38, L13406. https://doi.org/10.1029/2011GL047862.

Funk, C., Peterson, P., Landsfeld, M., Pedreros, D., Verdin, J., Rowland, J., Romero, B., Husak, G., Michaelsen, J. and Verdin, A. (2014) A quasi-global precipitation time series for drought monitoring. *US Geological Survey Data Series*, 832, 4. https://doi.org/10.3133/ds832.

Gloor, E., Wilson, C., Chipperfield, M.P., Chevallier, F., Buermann, W., Boesch, H., Parker, R., Somkuti, P., Gatti, L.V., Correia, C., Domingues, L.G., Peters, W., Miller, J., Deeter, M.N. and Sullivan, M.J.P. (2018) Tropical land carbon cycle responses to 2015/16 El Niño as recorded by atmospheric greenhouse gas and remote sensing data. *Philosophical Transactions of the Royal Society B*, 373, 20170302. https://doi.org/10.1098/rstb.2017.0302.

Gu, G. and Adler, R. (2019) Precipitation, temperature, and moisture transport variations associated with two distinct ENSO flavors during 1979-2014. *Climate Dynamics*, 52, 7249–7265.

Hill, K.J., Taschetto, A.S. and England, M.H. (2011) Sensitivity of south American summer rainfall to tropical Pacific Ocean SST anomalies. *Geophysical Research Letters*, 38, L01701. https://doi.org/10.1029/2010GL045571.

Hirahara, S., Balsameda, M.A., de Boisseson, E. and Hersbach, H. (2016) *Sea surface temperature and sea ice concentration for ERA5*. ERA Report Series 26, ECMWF Publications.

Jiménez-Muñoz, J.C., Mattar, C., Barichivich, J., Santamaría-Artigas, A., Takahashi, K., Malhi, Y., Sobrino, J.A., and van der Schrier, G. (2016) Record-breaking warming and extreme drought in the Amazon rainforest during the course of El Niño 2015-2016. *Scientific Reports*, 6, 33130. https://doi.org/10.1038/srep33130.

Jimenez-Muñoz, J.C., Barichivich, J., Mattar, C., Takahashi, K., Santamaría-Artigas, A., Sobrino, J.A. and Malhi, Y. (2018) Spatio-temporal patterns of thermal anomalies and drought over tropical forests driven by recent extreme climatic anomalies. *Philosophical Transactions of the Royal Society B*, 373. https://doi.org/10.1098/rstb.2017-0300.

Johnson, N.C. and Kosaka, Y. (2016) The impact of eastern equatorial Pacific convection on the diversity of boreal winter El Niño teleconnection patterns. *Climate Dynamics*, 47, 3737–3765. https://doi.org/10.1007/s00382-016-3039-1.

Kalnay, E., Kanamitsu, M., Kistler, R., Collins, W., Deaven, D., Gandin, L., Iredell, M., Saha, S., White, G., Woollen, J., Zhu, Y., Chelliah, M., Ebisuzaki, W., Higgins, W., Janowiak, J., Mo, K.C., Ropelewski, C., Wang, J., Leetmaa, A., Reynolds, R., Jenne, R. and Joseph, D. (1996) The NCEP/NCAR 40-year reanalysis project. *Bulletin of the American Meteorological Society*, 77(3), 437–472.

Kao, H.-Y. and Yu, J.-Y. (2009) Contrasting eastern-Pacific and Central-Pacific types of ENSO. *Journal of Climate*, 22(3), 615–632. https://doi.org/10.1175/2008JCLI2309.1.

Kendall, M.G. (1975) *Rank Correlation Methods*, 4th edition. London: Charles Griffin, p. 196.

Koren, G., van Schaik, E., Araújo, A.C., Folkert Boersma, K., Gärtner, A., Killaars, L., Kooreman, M. L., Kruijt, B., van der Laan-Luijkx, I.T., von Randow, C., Smith, N.E. and Peters, W. (2018) Widespread reduction in sun-induced fluorescence from the Amazon during the 2015/2016 El Niño. *Philosophical Transactions of the Royal Society B*, 373, 20170408.

L'Heureux, M.L., Takahashi, K., Watkins, A.B., Barnston, A.G., Becker, E.J., Di Liberto, T.E., Gamble, F., Gottschalck, J., Halpert, M.S., Huang, B., Mosquera-Vásquez, K. and Wittenberg, A.T. (2017) Observing and predicting the 2015/16 El Niño. *Bulletin of the American Meteorological Society*, 98(7), 1363–1382. https://doi.org/10.1175/BAMS-D-16-0009.1.

Liu, J., Bowman, K.W., Schimel, D.S., Parazoo, N.C., Jiang, Z., Lee, M., Bloom, A.A., Wunch, D., Frankenberg, C., Sun, Y., O'Dell, C.W., Gurney, K.R., Menemenlis, D., Gierach, M., Crisp, D. and Eldering, A. (2017) Contrasting carbon cycles responses of the tropical continents to the 2015-2016 El Niño. *Science*, 358. https://doi.org/10.1126/science.aam5690.

Luo, X., Keenan, T.F., Fisher, J.B., Jiménez-Muñoz, J.C., Chen, J.M., Jiang, C., Ju, W., Perakalapudi, N.-V., Ryu, Y. and Tadic, J.M. (2018) The impact of the 2015/2016 El Niño on global photosynthesis using satellite remote sensing. *Philosophical Transactions of the Royal Society B*, 373, 20170409.

Malhi, Y., Rowland, L., Aragao, L.E.O.C. and Fisher, R.A. (2018) New insights into the variability of the tropical land carbon cycle from the El Nino of 2015/2016. *Philosophical Transactions of the Royal Society B*, 373, 20170298. https://doi.org/10.1098/rstb.2017.0298.

Marengo, J.A., Nobre, C.A., Tomasella, J., Oyama, M.D., Sampaio de Oliveira, G., de Oliveira, R., Camargo, H., Alves, L.M. and Brown, I.F. (2008) The Drought of Amazonia in 2005. *Journal of Climate*, 21, 495–516. https://doi.org/10.1175/2007JCLI1600.1

Marengo, J.A., Alves, L.M., Soares, W.R. and Rodriguez, D.A. (2013) Two contrasting severe seasonal extremes in tropical South America in 2012: flood in Amazonia and drought in Northeast Brazil. *Journal of Climate*, 2, 9137–9154. https://doi.org/10.1175/JCLI-D-12-00642.1.

Marengo, J.A., Lincoln, M., Alvala, R.C.S., Cunha, A.P., Brito, S. and Moraes, O.L.L. (2018a) Climatic characteristics of the 2010-2016 drought in the semiarid Northeast Brazil region. *Annals of the*

Brazilian Academy of Sciences, 90, 1973–1985. https://dx.doi.org/10.1590/0001-3765201720170206

Marengo, J.A., Souza Carlos, M., Thonicke, K., Burton, C., Halladay, K., Betts, R.A., Alves, L.M. and Soares, W.R. (2018b) Changes in climate and land use over the Amazon region: current and future variability and trends. *Frontiers in Earth Science*, 6(228). https://doi.org/10.3389/feart.2018.00228.

Nogueira, S.M.C., Moreira, M.A. and Volpato, M.M.L. (2018) Evaluating precipitation estimates from eta, TRMM and CHRIPS data in the south-southeast region of Minas Gerais state-Brazil. *Remote Sensing*, 10, 313. https://doi.org/10.3390/rs10020313.

Paredes-Trejo, F.J., Barbosa, H.A. and Lakshmi Kumar, T.V. (2017) Validating CHIRPS-based satellite precipitation estimates in Northeast Brazil. *Journal of Arid Environments*, 139, 26–40. https://doi.org/10.1016/j.jaridenv.2016.12.009.

Paredes-Trejo, F.P., Barbosa, H.A. and Spatafora, L.R. (2018) Assessment of SM2RAIN-derived and state-of-the-art satellite rainfall products over Northeastern Brazil. *Remote Sensing*, 10, 1093. https://doi.org/10.3390/rs10071093.

Ropelewski, C. and Halpert, M. (1987) Global and regional scale precipitation patterns associated with the El Nino/southern oscillation. *Journal of Climate*, 115, 1606–1626.

Sen, P.K. (1968) Estimates of the regression coefficient based on Kendall's tau. *Journal of the American Statistical Association*, 63, 1379–1389.

Strahler, A., Muchoney, D., Borak, J., Friedl, M., Gopal, S., Lambin, E. and Moody, A. (1999). MODIS Land Cover Product. Algorithm Theoretical Basis Document 5.0, Boston University.

Sulca, J., Takahashi, K., Espinoza, J.-C., Vuille, M. and Lavado-Casimiro, W. (2018) Impacts of different ENSO flavors and tropical Pacific convection variability (ITCZ, SPCZ) on austral summer rainfall in South America, with a focus on Peru. *International Journal of Climatology*, 38(1), 420–435. https://doi.org/10.1002/joc.5185.

Takahashi, K., Montecinos, A., Goubanova, K. and Dewitte, B. (2011) ENSO regimes: reinterpreting the canonical and Modoki El Niño. *Geophysical Research Letters*, 38, L10704.

Tedeschi, R.G. and Collins, M. (2015) The influence of ENSO on south American precipitation during austral summer and autumn in observations and models. *International Journal of Climatology*, 36, 618–635. https://doi.org/10.1002/joc.4371.

Timmermans, A., An, S.-I., Kug, J.-S., Jin, F.-F., Cai, W., Capotondi, A., Cobb, K.M., Lengaigne, M., McPhaden, M.J., Stuecker, M.F., Stein, K., Wittenberg, A.T., Yun, K.-S., Bayr, T., Chen, H.-C., Chikamoto, Y., Dewitte, B., Dommenget, D., Grothe, P., Guilyardi, E., Ham, Y.-G., Hayashi, M., Ineson, S., Kang, D., Kim, S., Kim, W., Lee, J.-L., Li, T., Luo, J.-J., McGregor, S., Planton, Y., Power, S., Rashid, H., Ren, H.-L., Santoso, A., Takahashi, K., Todd, A., Wang, G., Wang, G., Xie, R., Yang, W.-H., Yeh, S.-W., Yoon, J., Zeller, E. and Zhang, X. (2018) El Niño-southern oscillation complexity. *Nature*, 559, 535. https://doi.org/10.1038/s41586-018-0252-6.

Zheleznova, I.V. and Gushchina, D.Y. (2017) Hadley and Walker circulation anomalies associated with the two types of El Niño. *Russian Meteorology and Hydrology*, 42(10), 625–634.

SUPPORTING INFORMATION

Additional supporting information may be found online in the Supporting Information section at the end of this article.

How to cite this article: Jimenez JC, Marengo JA, Alves LM, *et al.* The role of ENSO flavours and TNA on recent droughts over Amazon forests and the Northeast Brazil region. *Int J Climatol*. 2019;1–20. https://doi.org/10.1002/joc.6453